Convergence Analysis in Deterministic 3D Ray Launching Radio Channel Estimation in Complex Environments

L. Azpilicueta [1], M. Rawat [2], K. Rawat [2], F. Ghannouchi [2] and F. Falcone [1]

[1] Department of Electrical and Electronic Engineering
Public University of Navarre, Pamplona 31006, Spain
leyre.azpilicueta@unavarra.es, francisco.falcone@unavarra.es

[2] Department of Electrical and Computer Engineering
University of Calgary, Calgary, Alberta, Canada
mrawat@ucalgary.ca, krawat@ucalgary.ca, fghannou@ucalgary.ca

Abstract ─ In this paper, a convergence analysis to obtain the optimal calculation parameters in an in-house 3D ray launching algorithm to model the radio wave propagation channel in complex indoor environments is presented. Results show that these parameters lead to accurate estimations with reduced computational time. In addition, simulation results of an indoor complex scenario in terms of received power and power delay profile are presented, showing significant influence of multipath propagation in an indoor radio channel. The adequate election of simulation parameters given by convergence conditions, can aid in optimizing required computational time.

Index Terms – Convergence analysis, 3D ray launching, radio channel simulation, radio wave propagation.

I. INTRODUCTION

With the growing demand for wireless communication services in the last two decades, a radioplanning tasks for these systems is compulsory. Thus, a thorough analysis of indoor propagation channel characteristics represents a fundamental step toward the design and the implementation for an efficient setup of an indoor wireless network.

Traditionally, empirical methods were used (such as COST-231, Walfish-Bertoni, Okumura-Hata, etc.) for initial coverage estimation [1-3]. These empirical models can give rapid results but cannot take into account site-specific features, exhibiting limited accuracy. As an alternative, deterministic methods have been proposed [4-10] based on numerical approaches involving either solution of Maxwell's equations using full-wave simulation techniques, such as method of moment (MoM) and finite difference time domain (FDTD) [11]; or, using geometrical approximations such as Ray Launching (RL) [12] and Ray Tracing (RT) [13]. During the 1990s, RL and RT were both classified as ray tracing methods; although, more recently the differences between both methods have been distinguished. RL is based on the fact that a transmitter launches thousands of test rays in a solid angle and the true path is determined by searching for the rays arriving at the receiver; whereas, RT estimates the principal radio wave propagation regions and rays are traced in such regions. These methods are precise but are time-consuming due to inherent computational complexity. Their combination with Uniform Theory of Diffraction (UTD) [14] is frequently applied to radio coverage prediction [15-18]. RT and RL models potentially represent the most accurate and versatile methods for urban and indoor multipath propagation characterization. Nevertheless, the computational time in conventional ray launching defined by the Shooting-and-Bouncing-Ray (SBR) method [19], can be very large depending on the required accuracy of the results.

A prerequisite to the modeling of complex environments with standard computer equipment,

Submitted On: July 10, 2013
Accepted On: April 17, 2014

is an outstanding reduction of memory efforts with an accurate approach. In [20], Weinmann presents a new efficient approach in order to assess the simulation of scattered fields from arbitrary metallic objects with a ray tracing algorithm, which combines the principles of Physical Optics (PO) and the Physical Theory of Diffraction (PTD). This paper demonstrates that both CPU time and accurate results depend strongly on the number of rays N and the accuracy of the geometric model. The treatment of multiple interactions in a GO-PO approach has been studied in [21], showing that on one hand the multiple PO approach indeed is more accurate. On the other hand, the simulation efforts increase exponentially with the order of the reflection, which makes multiple PO not applicable to more than double reflections. In [22], a description of a novel implementation of diffracted rays according to the Uniform Theory of Diffraction (UTD) concept into a SBR code is presented, describing a convergence analysis with respect to the number of diffracted rays and in terms of multiple diffractions. In [23], a Geometrical Ray Implementation for Mobile Propagation Modeling (GRIMM) is presented, which splits the 3-D ray construction problem into two successive two-dimensional (2-D) stages, without loss of generality and with a great gain in time and simplicity. This permits to take into account reflections and diffractions in any order to meet convergence. In [24], a convergence analysis of a refined ray-tracing algorithm is carried out with respect to the propagation time and the number of bounces.

It is proved that an increase of the number of rays and angular resolution in a SBR approach achieves satisfying results but leads to the significant drawback of higher computational time [20]. Therefore, it is relevant to study the convergence of the results when using ray tracing methods.

In this work, an analysis of the convergence of an in-house developed 3D ray launching algorithm has been presented with respect to the computational time, the angular resolution of the shooting rays and the number of reflections considered. This code has been employed as an effective tool to analyze the effect of radio wave propagation in different complex environments [25-28]. Results show the optimal parameters to achieve the commitment between accuracy and computational time in radio wave simulations of complex indoor environments.

This paper is organized as follows: the in-house developed 3D ray launching code is analytically described in sections II and III. Section IV presents the considered scenario for the analysis and the convergence analysis of the algorithm, whereas simulation results of the algorithm are discussed in section V. Finally, conclusions are given in section VI.

II. THE RAY-LAUNCHING TECHNIQUE

As it is illustrated in Fig. 1, ray launching techniques are based on identifying a single point on the wave front of the radiated wave, with a ray that propagates along the space following a combination of optic and electromagnetic theories.

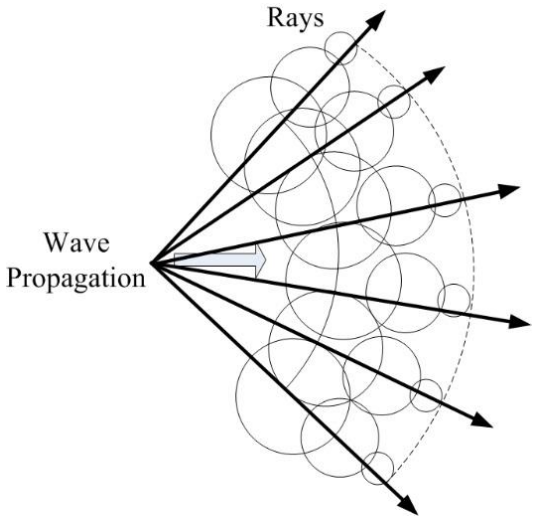

Fig. 1. Wave front propagation with rays associated with single wave front points.

Each ray propagates in the space as a single optic ray. The electric field E created by an antenna with a radiated power P_{rad}, with a directivity $D_t(\theta_t,\Phi_t)$ and polarization ratio $(X^{\perp}, X^{\parallel})$ at distance d in the free space is calculated by [29]:

$$E_i^{\perp} = \sqrt{\frac{P_{rad} D_t(\theta_t,\emptyset_t)\eta_0}{2\Pi}}\ \frac{e^{-j\beta_0 r}}{d}\ \mathrm{X}^{\perp} L^{\perp}, \quad (1)$$

$$E_i^{\parallel} = \sqrt{\frac{P_{rad} D_t(\theta_t,\emptyset_t)\eta_0}{2\Pi}}\ \frac{e^{-j\beta_0 r}}{d}\ \mathrm{X}^{\parallel} L^{\parallel}, \quad (2)$$

where $\beta_0 = 2\pi f_c\sqrt{\varepsilon_0\mu_0}$, ε_0=8.854*10^{-12}, μ_0=4π*10^{-7} and η_0=120π. $L^{\perp\parallel}$ are the path loss coefficients for each polarization.

When this ray finds an object in its path, two new rays are created: a reflected ray and a transmitted ray. These rays have new angles provided by Snell's law [30]. Once the parameters of transmission *T* and reflection *R* are calculated and the angle of incidence Ψ_i and Ψ_t, the new angles (θ_r,Φ_r) of the reflected wave and (θ_t,Φ_t) of the transmitted wave can be calculated. A general case where a ray impinges with an obstacle with (θ_i',Φ_i') angles, is represented in Fig. 2. Taking into account all the possible angles of incidence, the new angles for the reflected and transmitted wave are calculated, as it is shown for a general case in Fig. 2.

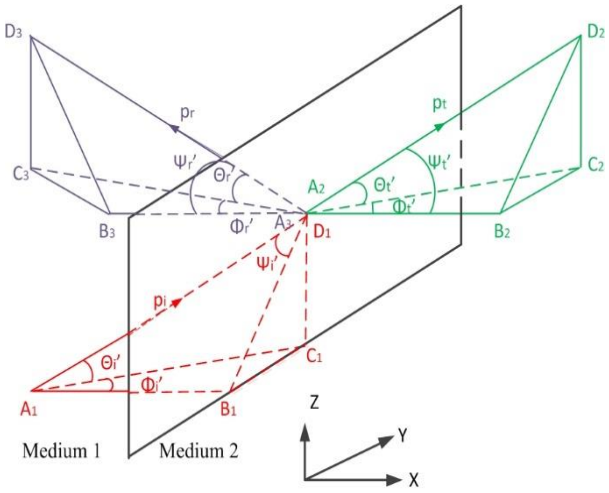

Fig. 2. Reflection and transmission by plane interface at the oblique wave incidence.

The diffracted field is calculated by [31]:

$$E_{UTD} = e_0 \frac{e^{-jks_1}}{s_1} D^{\perp\parallel} \sqrt{\frac{s_1}{s_2(s_1+s_2)}}\, e^{-jks_2}, \quad (3)$$

where s_1, s_2 are the distances represented in Fig. 3, from the source to the edge and from the edge to the receiver point. $D^{\perp\parallel}$ are the diffraction coefficients in (4) given by [31-33] as:

$$D^{\parallel\perp} = \frac{-e^{(-j\pi/4)}}{2n\sqrt{2\pi k}} \left\{ \begin{array}{l} \cot\left(\frac{\pi+(\Phi_2-\Phi_1)}{2n}\right) F\left(kLa^+(\Phi_2-\Phi_1)\right) \\ +\cot\left(\frac{\pi-(\Phi_2-\Phi_1)}{2n}\right) F\left(kLa^-(\Phi_2-\Phi_1)\right) \\ +R_0^{\parallel\perp}\cot\left(\frac{\pi-(\Phi_2+\Phi_1)}{2n}\right) F\left(kLa^-(\Phi_2+\Phi_1)\right) \\ +R_n^{\parallel\perp}\cot\left(\frac{\pi+(\Phi_2+\Phi_1)}{2n}\right) F\left(kLa^+(\Phi_2+\Phi_1)\right) \end{array} \right\}, \quad (4)$$

where nπ is the wedge angle, *F*, *L* and $a^{\pm}$ are defined in [31], and $R_{0,n}$ are the reflection coefficients for the appropriate polarization for the 0 face or n face, respectively. The Φ_2 and Φ_1 angles in (4) would refer to the angles in Fig. 3.

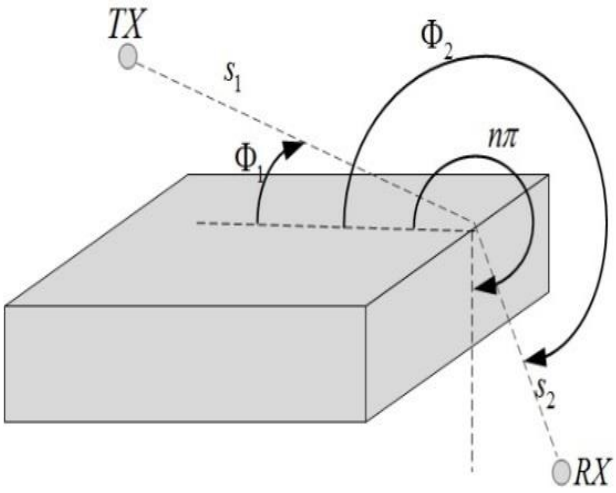

Fig. 3. Geometry for wedge diffraction coefficients.

The received power is calculated at each point taking into account the losses of propagation through a medium (ε, μ, σ) at a distance *d*, with the attenuation constant α (Np/m) and the phase constant β (rad/m). The received power is calculated with the sum of incident electric vector fields in an interval of time Δ_t inside each cuboid of the defined mesh. Based on the above theory, the main characteristic of the ray-launching technique is that it provides the impulse response of the channel *h* (*t*, *fc* , *Δf, d*) for each transmitter, at a given carrier frequency, *fc*, at a given bandwidth (*fc* ± *Δf*), where the materials have a similar response and at a given position. With this information, a stationary channel can be wholly characterized.

III. THE 3D RAY-LAUNCHING ALGORITHM

The developed in-house 3D ray-launching algorithm has three phases:

- Phase I: Scenario creation
- Phase II: 3D ray-launching simulation
- Phase III: Analysis results

In phase I, the 3D scenario is created by considering several objects, walls, transmitters, receivers and the whole components of the environment. It is important to emphasize that a grid is defined in the space to save the parameters of each ray. Accordingly, the environment is divided into a number of cuboids of a fixed size. When a ray enters a specific hexahedron, its parameters are saved in a matrix. Parameters such as frequency of operation, radiation patterns of the antennas, number of multipath reflections, separation angle between rays and cuboid dimension can be modified in the algorithm. In order to achieve adequate values, it is highly important to take into account, not only the parameters which result in more accurate results, but also the computational time, which can be substantial for a complex environment.

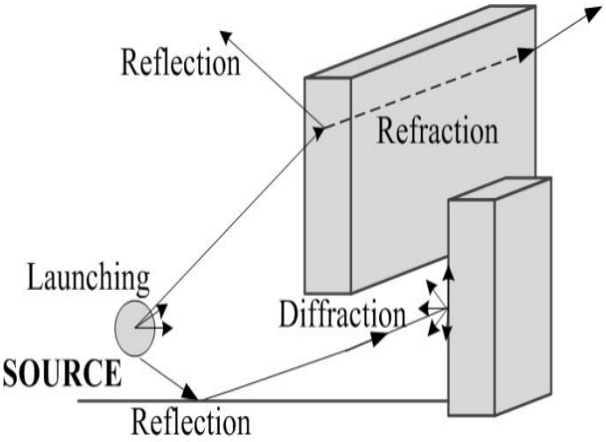

Fig. 4. Principle of operation of the in-house developed 3D ray launching code.

In phase II, rays are launched and they propagate along the space interacting with the obstacles, causing physical phenomena such as reflection, refraction and diffraction, as shown in Fig. 4. The parameters of these rays are stored as they enter to each hexahedral until the ray has a certain number of reflections or it has exceeded the pre-propagation time set. The algorithm operates in an iterative manner, considering a ray and its reflections and storing the created ray for processing later the diffraction contribution. Figure 5 shows the different steps of this phase of the algorithm.

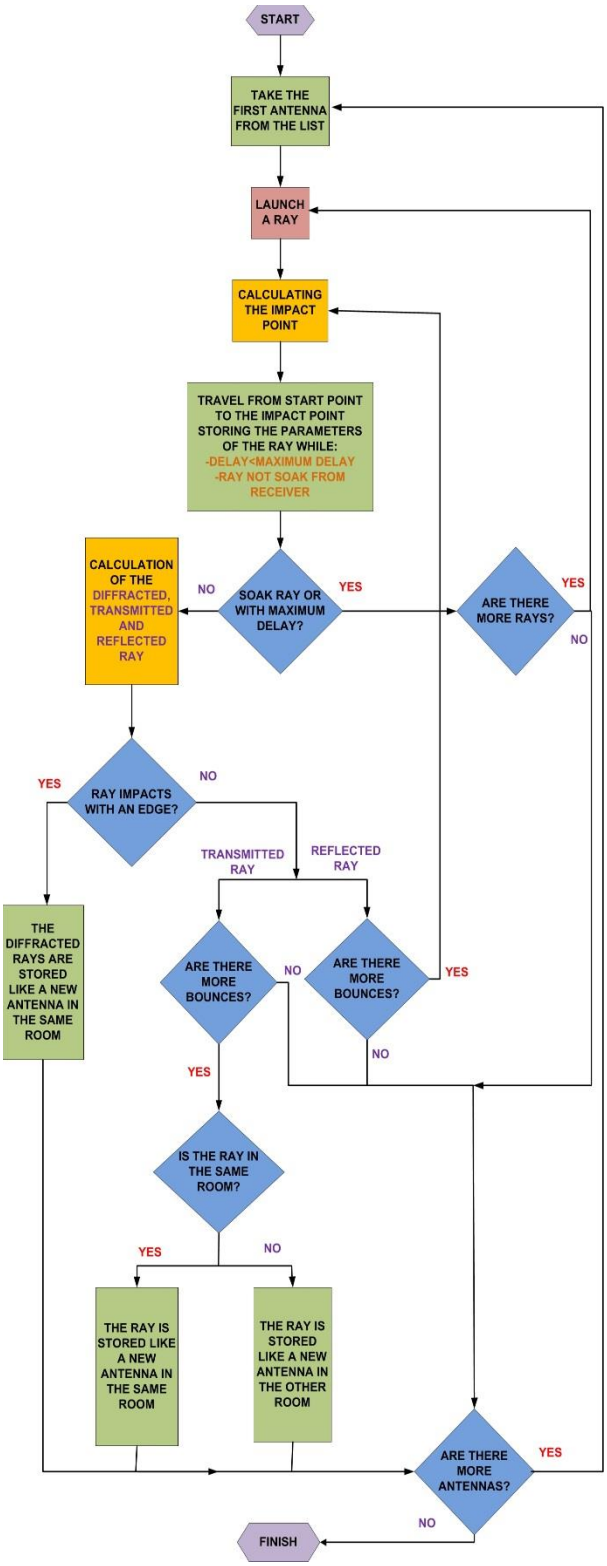

Fig. 5. Functional diagram of the 3D ray launching algorithm.

In phase III, by using the parameters stored in phase II and considering the predefined transmitter's characteristics, such as radiated power, the emitting antenna's directivity *(θ,Φ),* wave polarization and the carrier frequency, it is possible to easily derive the relevant parameters for channel modeling.

IV. CONVERGENCE ANALYSIS

In principle, it can be stated that simulation results tend to be more accurate whether more rays are launched and more reflections are considered. However, computational time has to be taken into account in order to obtain accurate results with an acceptable time span.

In this work, the influence of considering a different number of reflections and launching rays has been done. For that purpose, two different angular resolutions of launching rays have been considered and analyzed, versus the number of reflections. Afterwards, once the optimal number of reflections has been obtained, the assessment of the most accurate angular resolution of launching rays has been done taking into account the computational time.

The scenario under consideration is a complex environment, which corresponds to several rooms of the iRadio Laboratory of the University of Calgary. A schematic view of the scenario is represented in Fig. 6.

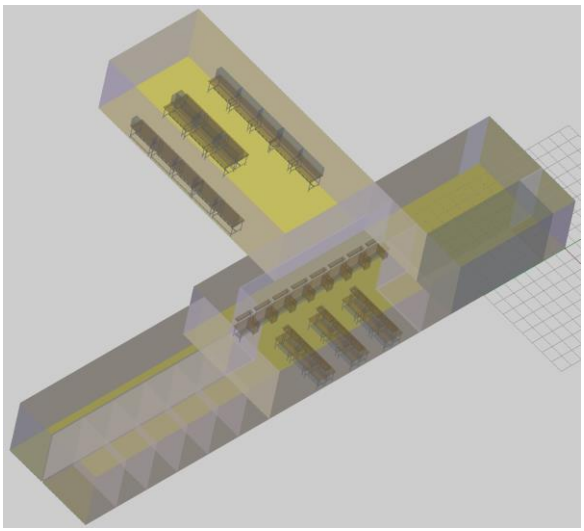

Fig. 6. Complete scenario of iRadio Laboratory of the University of Calgary.

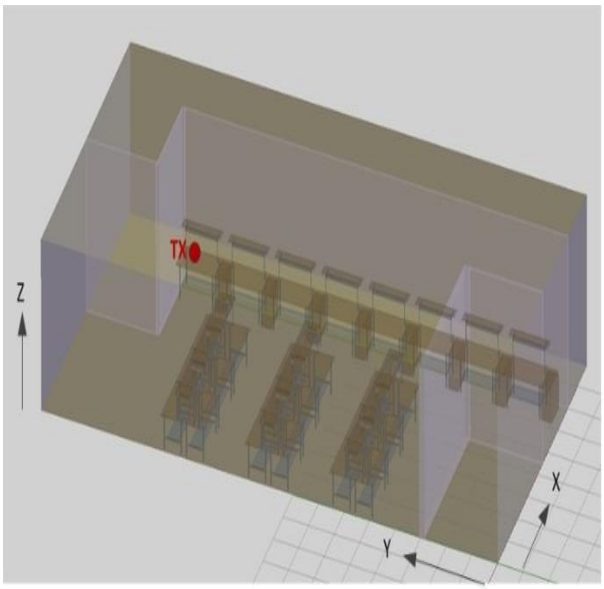

Fig. 7. Detail of room 2 of the complete scenario representing the iRadio Laboratory.

Within the complete scenario, only one room has been chosen to analyze exhaustively, room 2, which is depicted in detail in Fig. 7. The red point in this figure corresponds to the transmitter antenna, which is placed at the point (X=6.24 m, Y=16.94 m and Z=0.96 m). All the elements within the scenario have been taking into account (i.e. the different dimension and distribution of tables and chairs and walls). The material parameters used in the simulation models are defined in Table 1 [34].

Table 1: Material parameter definition

Material Properties in the Ray Launching Simulation		
Material	Permittivity (ε_r)	Conductivity $(\sigma)[S/m]$
Air	1	0
Aluminum	4.5	$4*10^7$
Glass	6.06	10^{-12}
Wood	3	0.0006
Brick wall	5.2	0.028

A. Convergence versus the number of reflections

First, a convergence analysis of the algorithm versus the number of reflections that the ray could impact with the obstacles and walls has been

obtained. Different cases have been considered varying the number of reflections. These cases correspond to different angular resolutions when the rays are launched, as shown in Table 2.

Table 2: Different cases considered for simulation versus the number of reflections

	$N_{launching\ rays}$	$\Delta\Phi=\Delta\theta$
Case 0	16200	2º
Case 1	64800	1º
Case 2	259200	0.5º

Table 3: Simulation parameters

Ray Launching Parameters	
Frequency	2.4 GHz
Transmitter power	20 dBm
Cuboids resolution	12x12x12 cm
Transmitter point	(X=6.24 m,Y=16.94 m and Z=0.96 m)

Case 1 and case 2 have been analyzed versus the number of reflections and simulation, parameters for both cases are shown in Table 3.

Figures 9, 10, 11 and 12 depict simulation results for case 1. The mean value and the standard deviation of power (dBm) for different X and Z and along the Y-axis are presented. These linear radials correspond to the red lines in Figs. 8 (a) and (b). The mean power values exhibits large variability, due to the influence of the morphology and topology of the scenario. Therefore, the way in which the elements within the indoor scenario are configured and the different material properties play a fundamental role in the overall performance of the network.

The standard deviation of power decreases as the number of reflections increases and converges approximately for six reflections in all cases, which implies that the maximum efficiency of the algorithm will be reached when six reflections are considered.

Figure 10 shows the linear regression lines of the received power for different locations in the X axis, along the Y-axis and for different heights. It is demonstrated that when the number of reflections considered in the algorithm has been increased, the algorithm tends to converge and it exhibits the same behavior from a threshold value for the number of reflections, corresponding to six reflections. In all cases, the trend is to decrease over distance and it is observed that with more reflections the slope of the lines is smaller.

Figure 11 shows the mean and the standard deviation of power (dBm) for different Y and Z locations and along the X-axis (green lines in Fig. 8 (a)). It is observed that mean power converges as the number of reflections increases. Besides, the standard deviation of the received power decreases and also converges at approximately six reflections.

Figure 12 shows the linear regression lines of the received power for different values in Y axis and heights and along the X-axis. It is observed that for smaller values in the Y axis, the slope of the lines is smaller as the number of reflections increases. From Y=6 m, figures of smaller heights show more variability due to the obstacles within the ray path. Lines converge as the number of reflections is increased. From Y=12 m, power increases along the X-axis due to the proximity of the transmitter antenna.

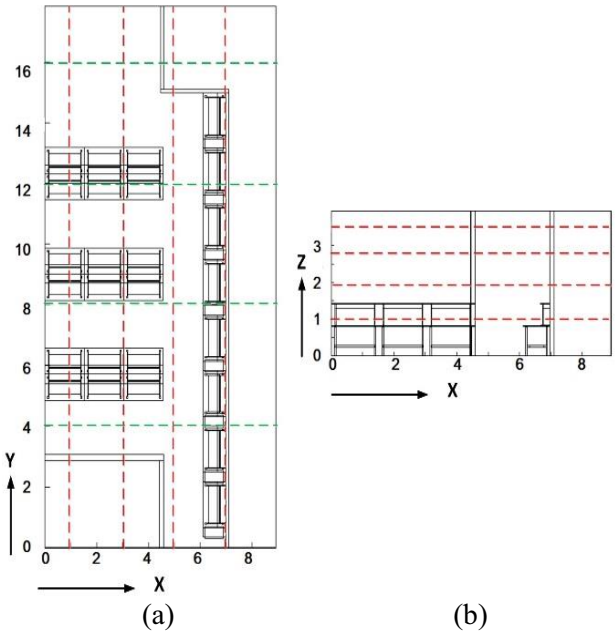

(a) (b)

Fig. 8. Schematic representation of the linear TX-RX distances chosen for the convergence analysis of the algorithm: (a) along the X-axis and the Y-axis and (b) different heights in the Z-axis.

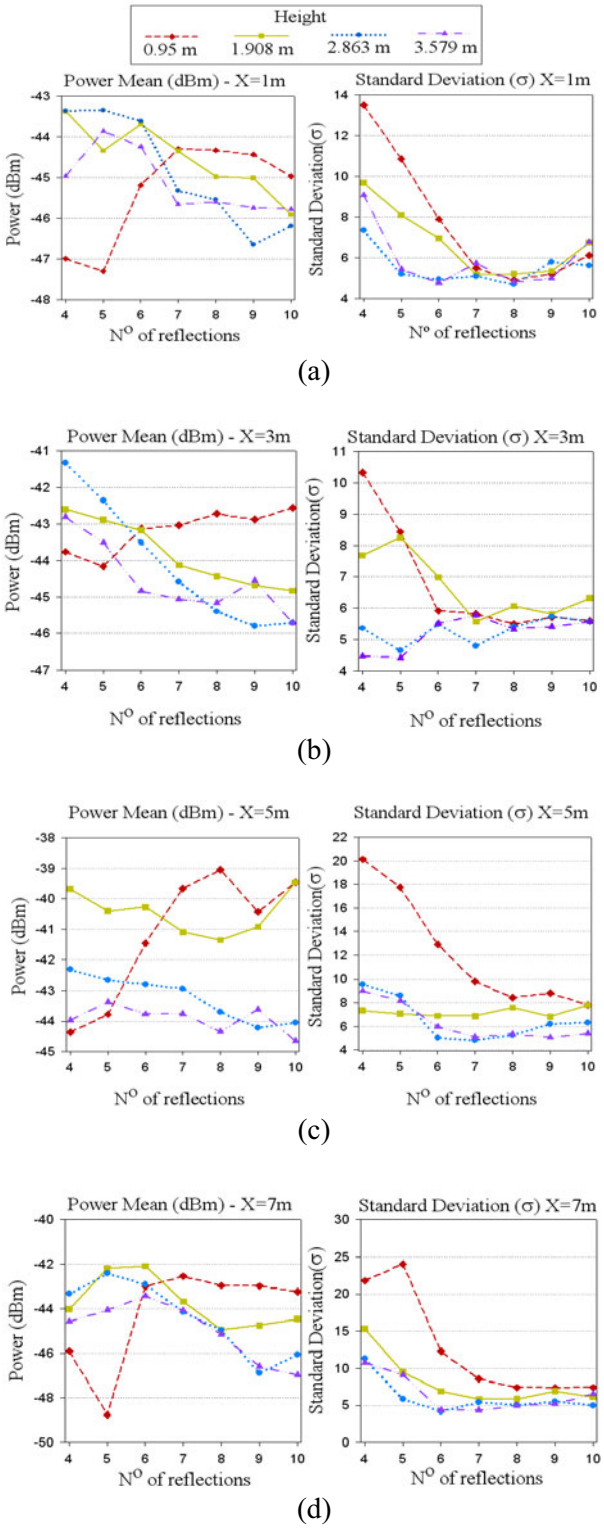

Fig. 9. Mean and standard deviation of power for different X and Z versus the number of reflections with $N_{launching\ rays}$=64800: (a) X=1 m, (b) X=3 m, (c) X=5 m and (d) X=7 m.

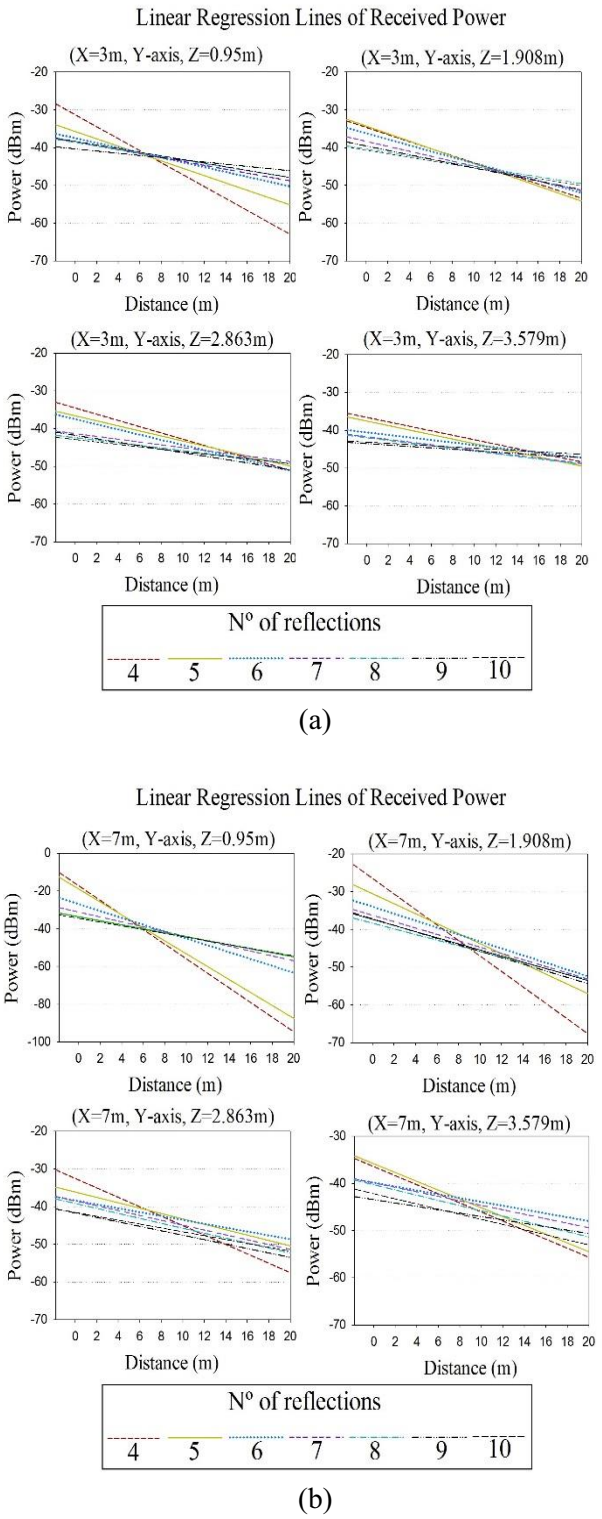

Fig. 10. Linear regression lines of the received power for different X, along the Y-axis and for different heights with $N_{launching\ rays}$=64800: (a) X=3 m and (b) X=7 m.

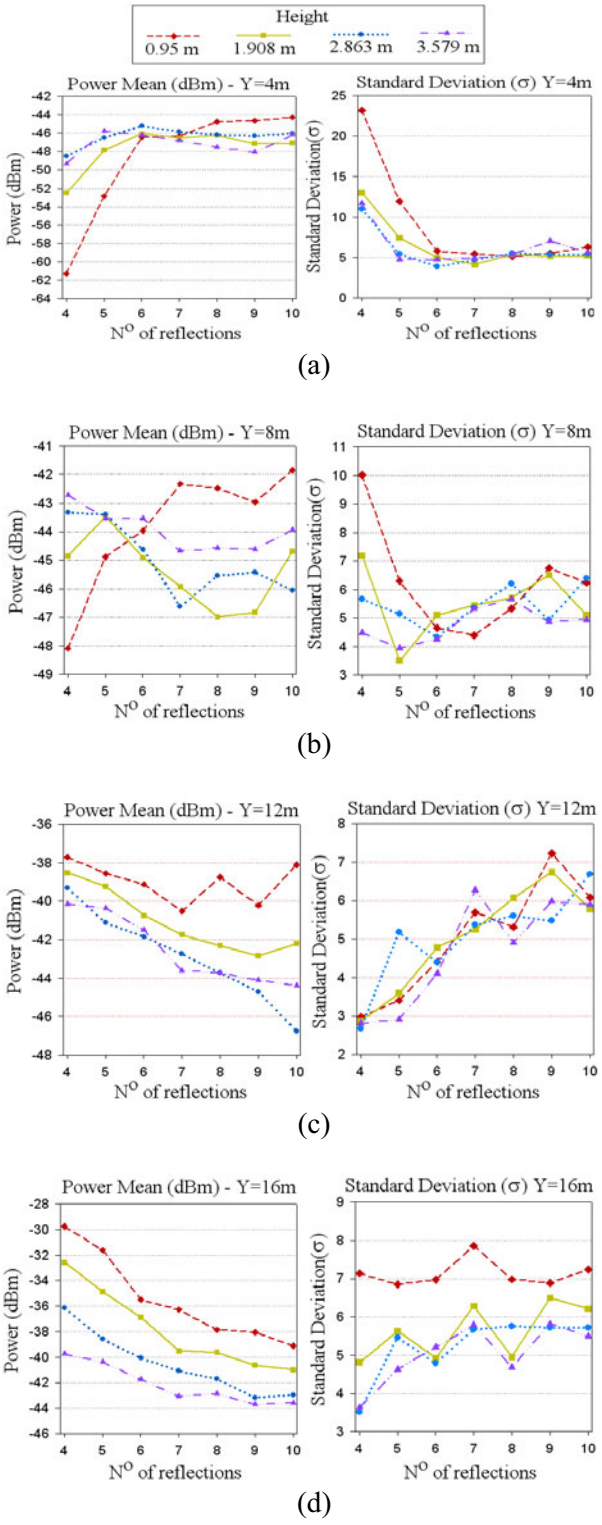

Fig. 11. Mean and standard deviation of power for different Y and Z versus the number of reflections with $N_{launching\ rays}$=64800: (a) Y=4 m, (b) Y=8 m (c) Y=12 m and (d) Y=16 m.

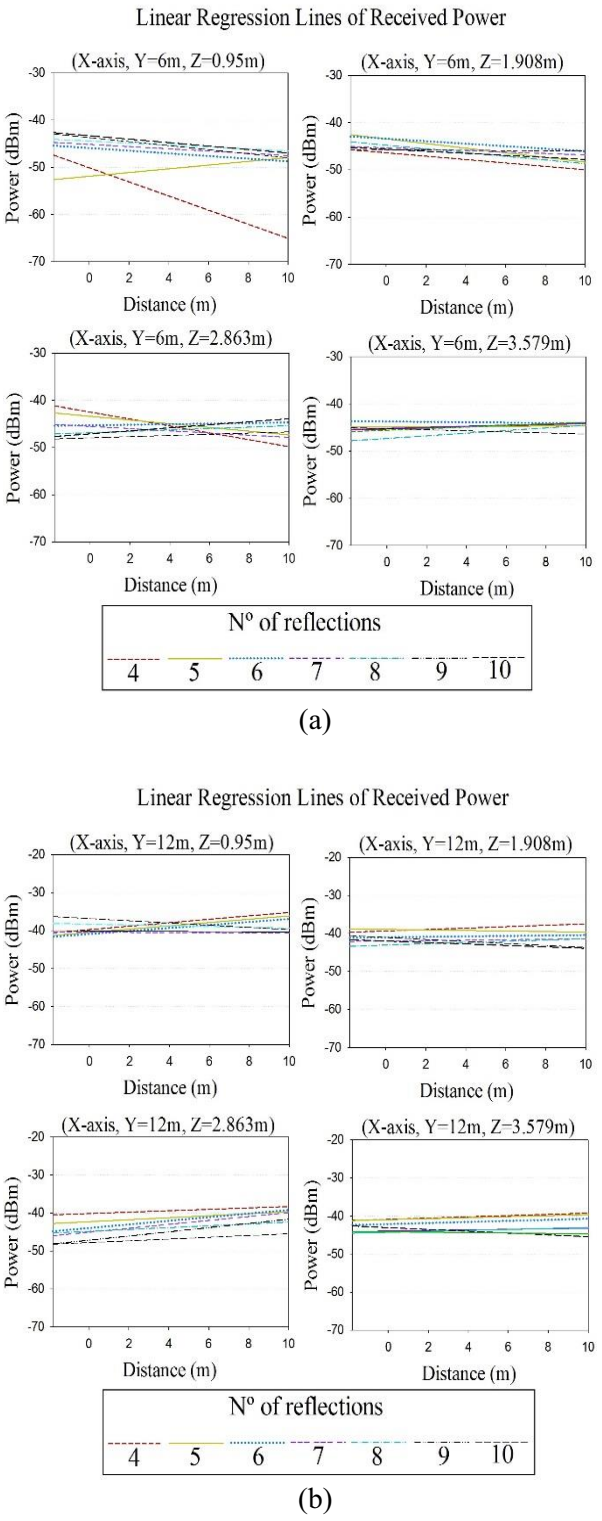

Fig. 12. Linear regression lines of the received power for different Y, along the X-axis and for different heights with $N_{launching\ rays}$=64800: (a) Y=6 m and (b) Y=12 m.

In order to validate previous results, which conclude that six reflections must be considered in complex indoor scenarios, the same analysis has been done with a lower angular resolution (case 2 in Table 2). This implies that the number of shooting rays is increased to test if the number of rays has an influence in the algorithm convergence. Simulation parameters are shown in Table 3.

Figure 13 represents the mean and the standard deviation of power (dBm) for different X and Z, along the Y-axis, with $\Delta\ \Phi = \pi/360$ and $\Delta\theta = \pi/360$. As in the previous case, large variability in the mean of the received power is observed, due to the influence of the morphology and topology of the scenario and multipath fading, which is a relevant phenomenon in this type of indoor scenarios. The standard deviation of the power does not converge as clearly as in the previous case. However, Figs. 13 (b) and (d) depict convergence of the algorithm.

The linear regression lines of the received power for different X, along the Y-axis and for different heights with angular resolution of launching rays of 0.5º, are presented in Fig. 14. It is observed that in all cases the received power decreases with the distance and the slope of the lines are smaller as the number of reflections increases. In case 2, the algorithm converges with one reflection less considered because of the rise of launching rays. The slope of the regression lines in Figs. 14 and 16 are for every height, smaller than case 1; therefore, the number of considered reflections to achieve the convergence is smaller.

However, the computational time is also deeply important. Simulations have been performed in an Intel Xeon CPU X5650 @ 2.67 GHz and 2.66 GHz. In case 2, the computational complexity is increased overall. Figure 17 shows the simulation time of the considered scenario depending on the number of reflections and the number of launching rays. Computational time with angular resolution of 0.5º (case 2) is hugely greater than case 1, with angular resolution of 1º for each number of reflections considered. It can be seen that the optimal parameters to achieve the most accurate results with an acceptable computational time, is to consider six reflections and angular resolution of launching rays of 1º.

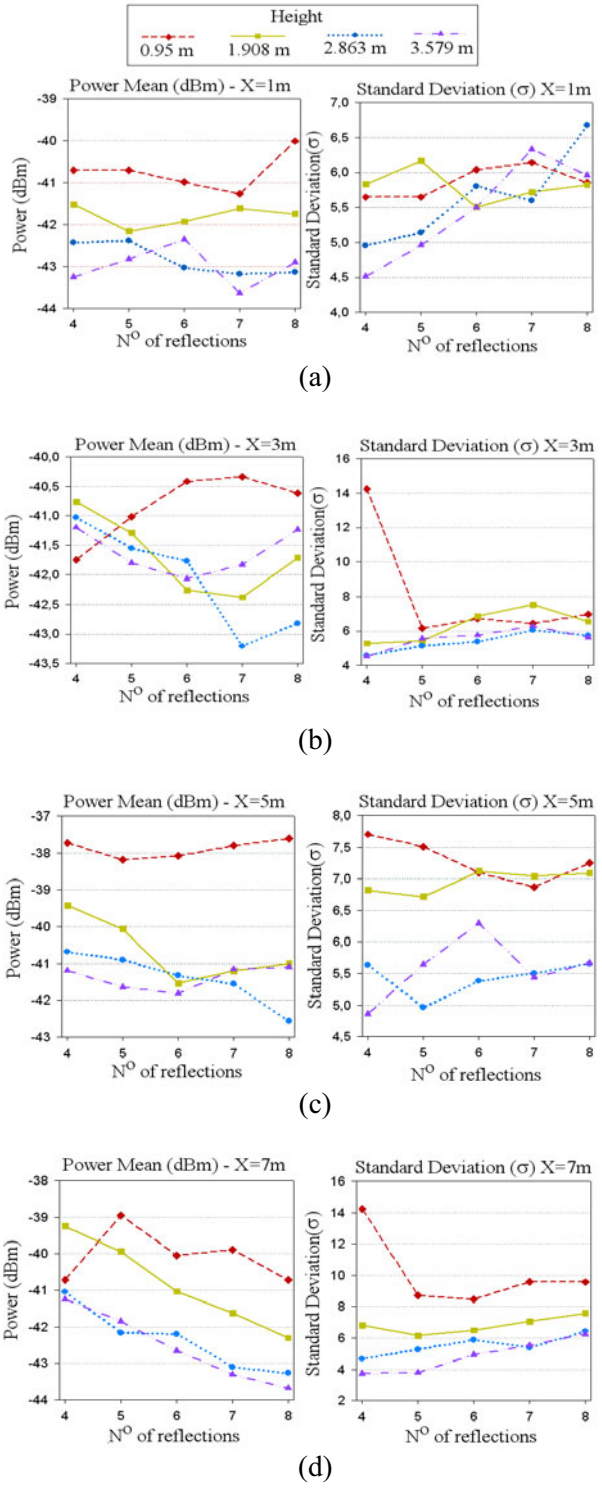

Fig. 13. Mean and standard deviation of power for different X and Z versus the number of reflections with $N_{launching\ rays}$=259200: (a) X=1 m, (b) X=3 m, (c) X=5 m and (d) X=7 m.

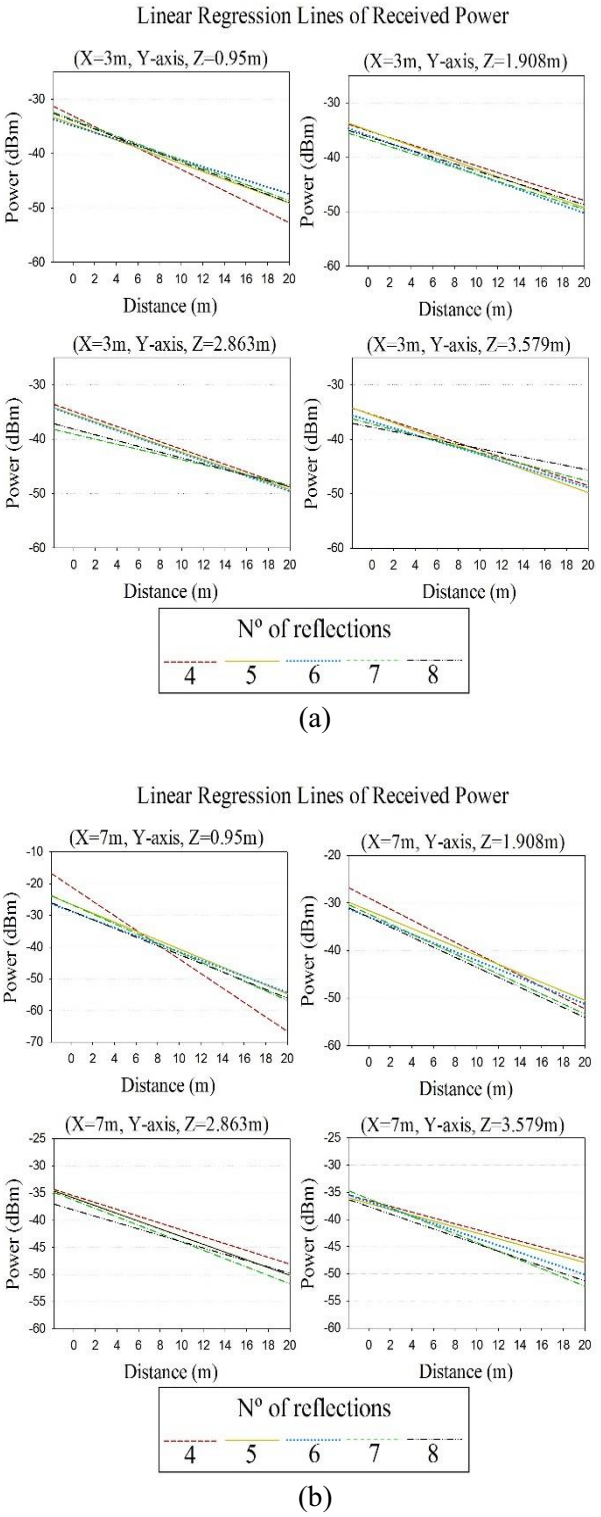

Fig. 14. Linear regression lines of the received power for different X, along the Y-axis and for different heights with $N_{launching\ rays}$=259200: (a) X=3 m and (b) X=7 m.

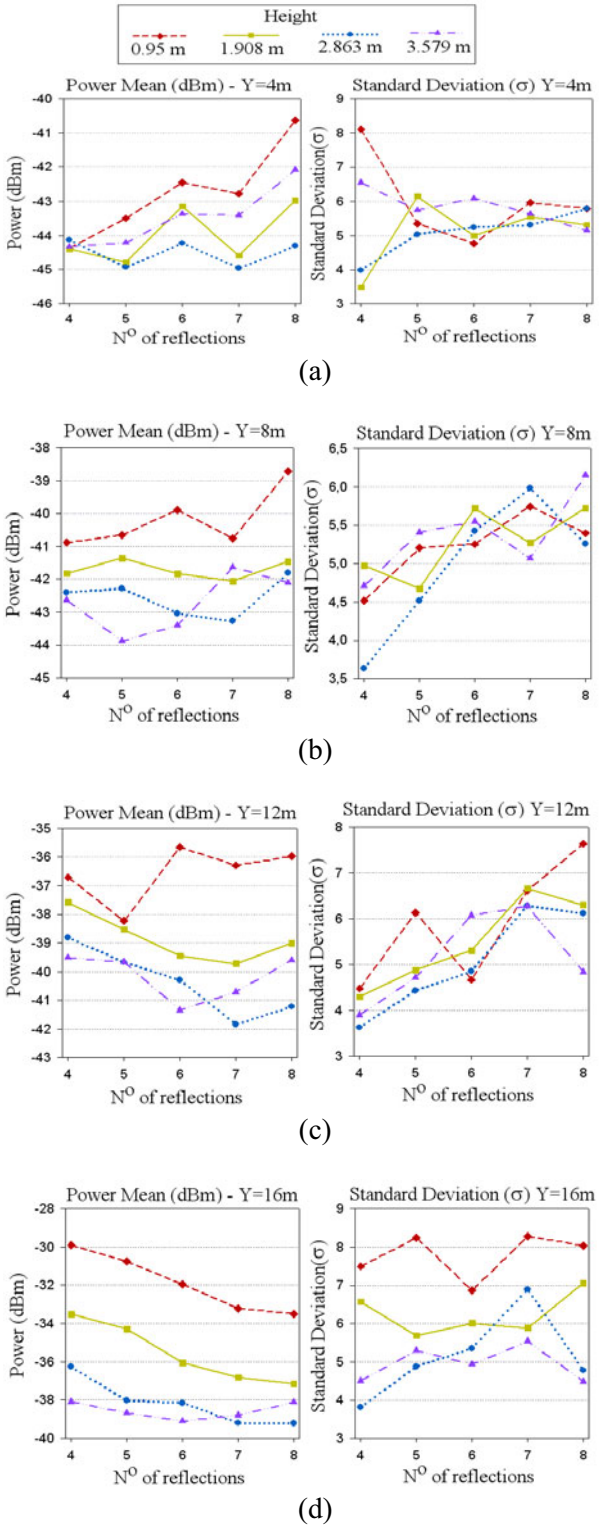

Fig. 15. Mean and standard deviation of power for different Y and Z versus the number of reflections with $N_{launching\ rays}$=259200: (a) Y=4 m, (b) Y=8 m, (c) Y=12 m and (d) Y=16 m.

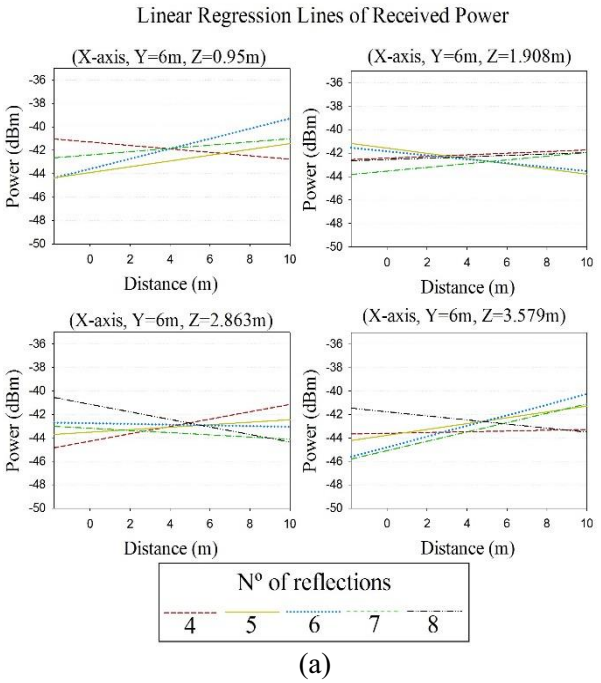

(a)

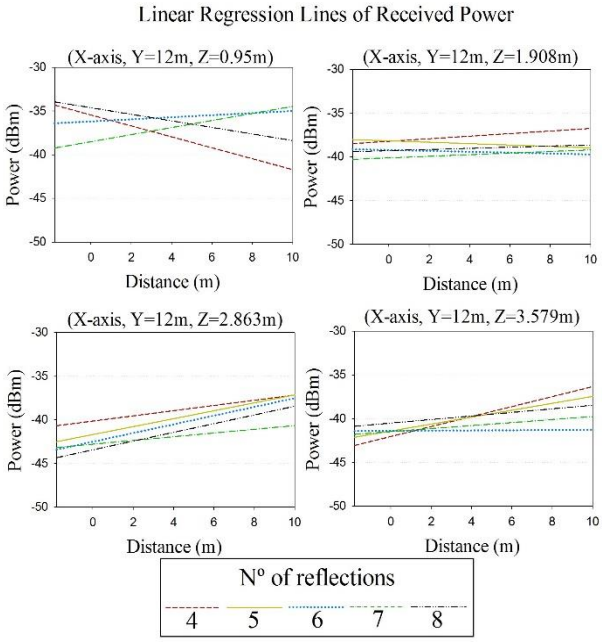

(b)

Fig. 16. Linear regression lines of the received power for different Y, along the X-axis and for different heights with $N_{launching\ rays}$=259200: (a) Y=6 m and (b) Y=12 m.

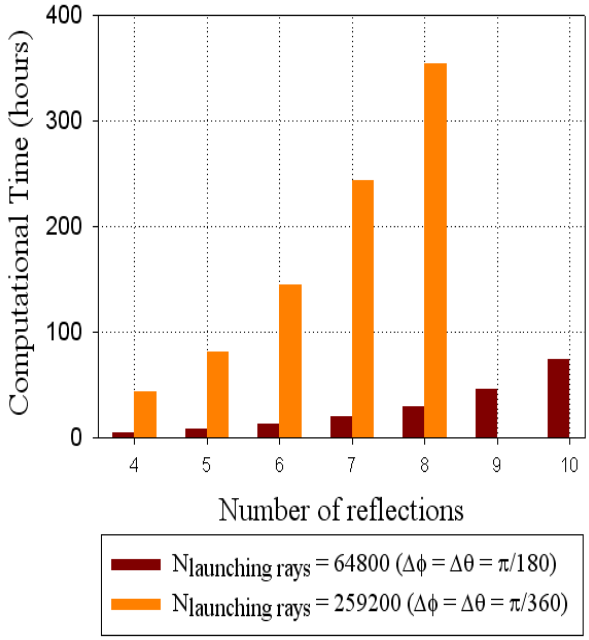

Fig. 17. Comparison of computational time versus different number of launching rays and different number of reflections considered in the algorithm.

B. Convergence versus the number of launching rays

In order to validate the results obtained in the previous section, an analysis of the convergence of the algorithm versus the number of launching rays has been performed considering six reflections. Figures 18 and 19 show the mean and the standard deviation of power for different locations in the X, Y axes and heights, in comparison with the three cases shown in Table 2. It can be seen that mean value of received power increases as the number of shooting rays is increased, which is in agreement with previous results in the sense that the algorithm is more accurate with more shooting rays. Alternatively, the standard deviation of power decreases sharply for case 0 to case 1, and converges in all cases in case 1, which corresponds to angular resolutions of 1º. Accordingly, these results validate the previous statements taking into account the high amount of CPU-time required to analyze the large amount of rays of case 3, which is shown in Fig. 20.

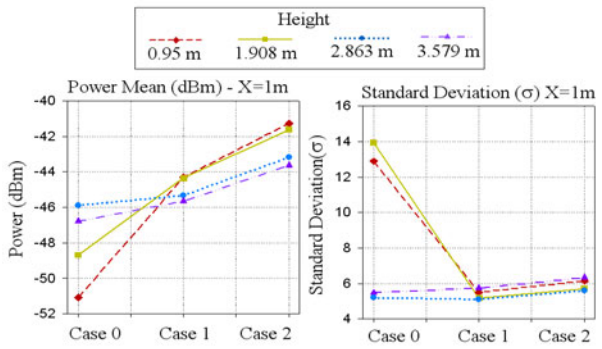

(a)

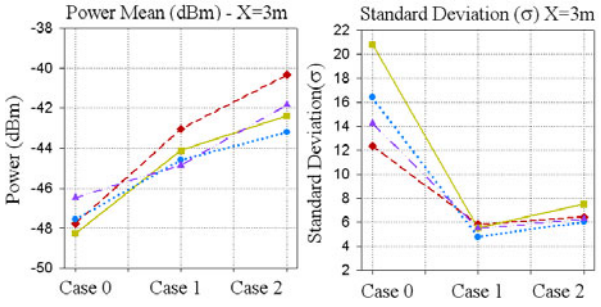

(b)

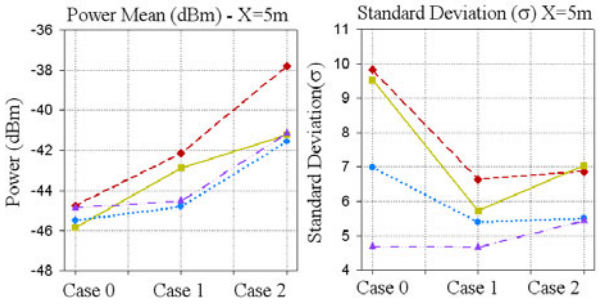

(c)

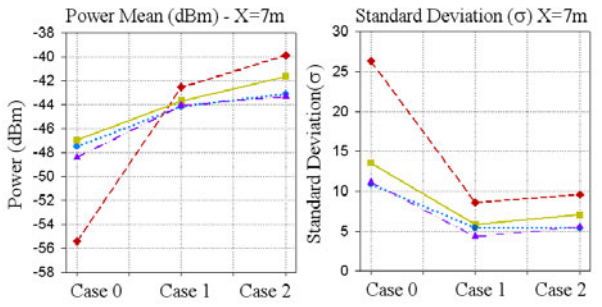

(d)

Fig. 18. Mean and standard deviation of power in room 2 versus different cases of shooting rays for different X.

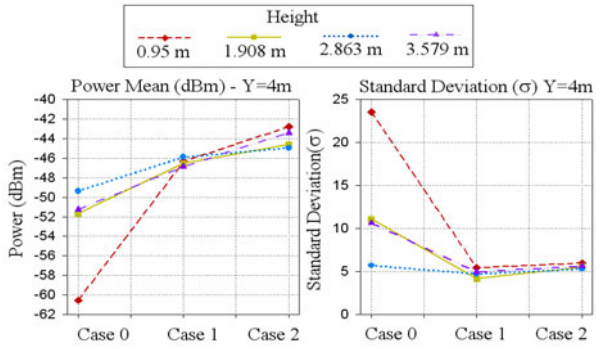

(a)

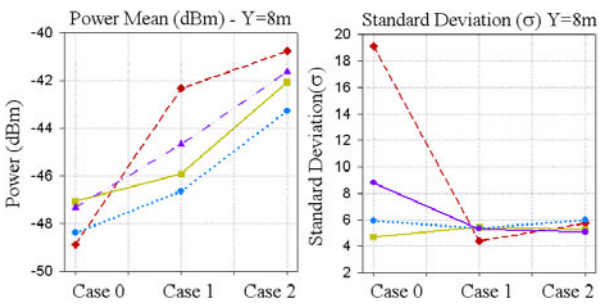

(b)

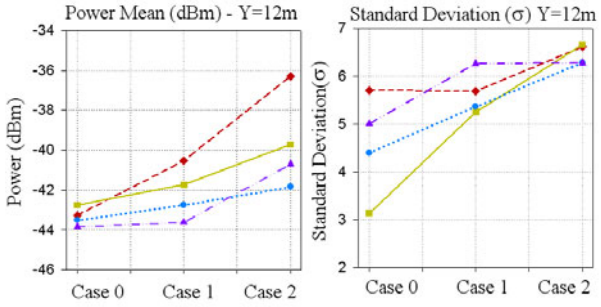

(c)

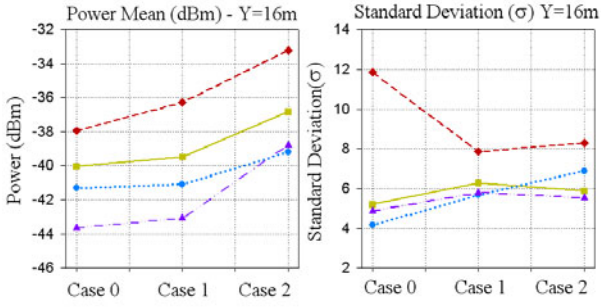

(d)

Fig. 19. Mean and standard deviation of power in room 2 versus different cases of shooting rays for different Y.

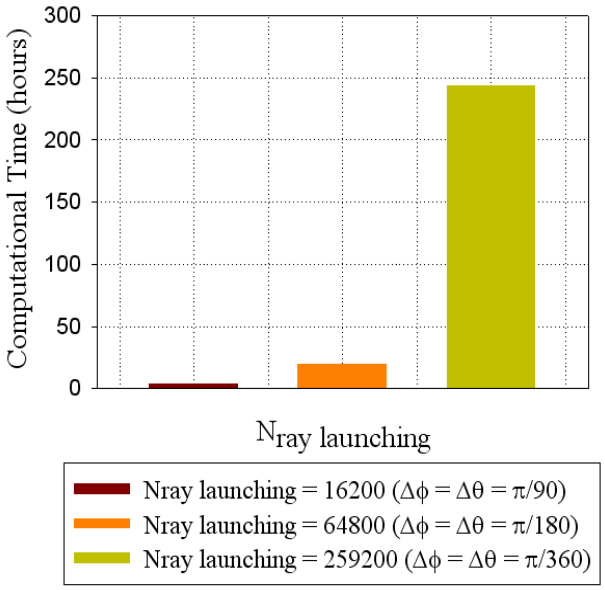

Fig. 20. Comparison of computational time versus different number of launching rays.

V. SIMULATIONS RESULTS

In order to gain insight in the effect of parameter variation in wireless channel estimation, several test cases have been simulated. Figure 21 shows the estimated received power for two different heights in the indoor scenario of the iRadio Laboratory (depicted in Fig. 7). Simulations have been performed with the parameters shown in Table 3, with an angular resolution of one degree and six reflections.

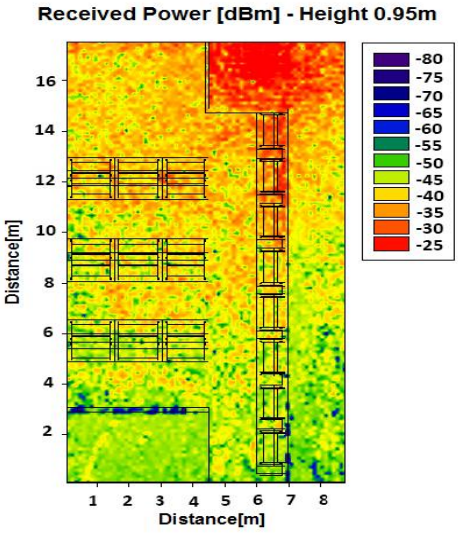

(a)

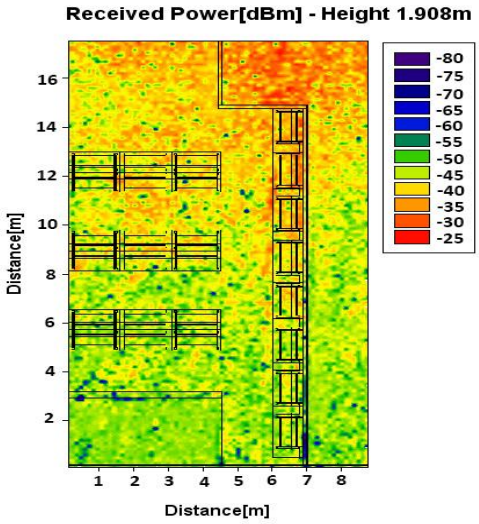

(b)

Fig. 21. Bi-dimensional planes of estimated received power: (a) hight 0.95 m and (b) height 1.908 m.

To illustrate the relevance of the multipath effect, the power delay profile has been predicted along for x=3 m, y=12 m and z=1.908 m, as shown in Fig. 22. It can be seen that there are a large number of echoes in the scenario, due to multipath propagation, which is the most important phenomena in this type of indoor scenarios.

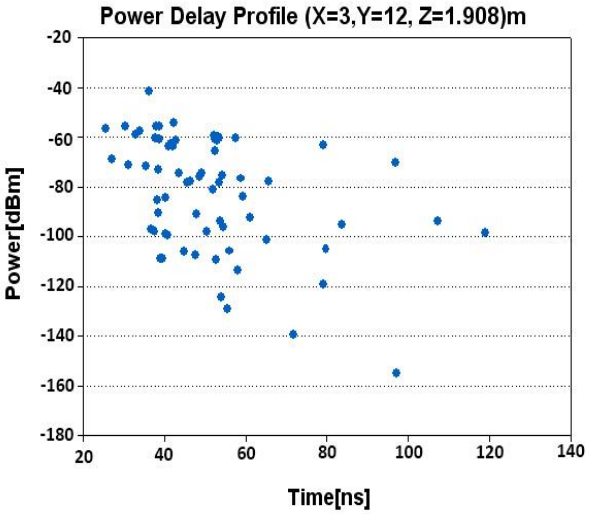

Fig. 22. Power-delay profile for: x=3 m, y=12 m and z=1.908 m, in the considered scenario.

VI. CONCLUSION

In this work, the convergence analysis to obtain the optimal parameters to introduce in a 3D in-house implemented ray launching code have been presented. Results show that adequate election of parameters such as ray angular resolution, number of reflections and cuboid resolution, lead to accurate results with adequate computational time as a consequence of algorithm convergence. In addition, simulation results of an indoor complex scenario in terms of received power and power delay profile are presented, showing the significant influence of multipath propagation in an indoor radio channel. These results can aid in the correct development of radioplanning tasks with optimal computational time.

ACKNOWLEDGMENT

The authors wish to acknowledge the financial support of project TEC2010-21563-C02-01 ENEIDA, funded by the Ministry of Science, Spain.

REFERENCES

[1] M. Hata, "Empirical formula for propagation loss in land mobile radio services," *IEEE Trans. Antennas and Propag*., vol. 29, no. 3, pp. 317-325, 1980.

[2] F. Ikegami, S. Yoshida, T. Takeuchi and M. Umehira, "Propagation factors controlling mean field strength on urban streets," *IEEE Trans. Antennas and Propa*g., vol. 32, no. 8, pp. 822-829, 1984.

[3] S. Phaiboon and P. Phokharatkul, "Path loss prediction for low-rise buildings with image classification on 2-D aerial photographs," *Progress in Electromagnetics Research*, vol. 95, pp. 135-152, 2009.

[4] S. H. Lee, "A photon modeling method for the characterization of indoor optical wireless communication," *Progress in Electromagnetics Research*, vol. 92, pp. 121-136, 2009.

[5] D. J. Y. Lee and W. C. Y. Lee, "Propagation prediction in and through buildings," *IEEE Trans. Veh. Tech*., vol. 49, no. 5, pp. 1529-1533, 2000.

[6] S. Y. Tan and H. S. Tan, "A microcellular communications propagation model based on the uniform theory of diffraction and multiple image theory," *IEEE Trans. Antennas and Propag*., vol 44, no. 10, pp. 1317-1326, 1996.

[7] A. G. Kanatas, I. D. Kountouris, G. B. Kostaras and P. Constantinou, "A UTD propagation model in urban microcellular environments," *IEEE Trans. Veh. Tech*., vol. 46, no. 1, pp. 185-193, 1997.

[8] A. G. Dimitriou and G. D. Sergiadis, "Architectural features and urban propagation," *IEEE Trans. Antennas and Propag*., vol. 54, no. 3, pp. 774-784, 2006.

[9] M. Franceschetti, J. Bruck and L. J. Schulman, "A random walk model of wave propagation," *IEEE Trans. Antennas and Propag*., vol. 52, no. 5, pp. 1304-1317, 2004.

[10] J. Blas Prieto, R. M. Lorenzo Toledo, P. Fernández Reguero, E. J. Abril, A. Bahillo Martínez, S. Mazuelas Franco and D. Bullido, "A new metric to analyze propagation models," *Progress in Electromagnetics Research*, vol. 91, pp. 101-121, 2009.

[11] J. W. Schuster and R. J. Luebbers, "Comparison of GTD and FDTD predictions for UHF radio wave propagation in a simple outdoor urban environment," *IEEE Antennas and Propag. Society International Symposium*, vol. 3, pp. 2022-2025, 1997.

[12] S. Y. Seidel and T. S. Rappaport, "Site-specific propagation prediction for wireless in-building personal communication system design," *IEEE Transactions on Vehicular Technology*, vol. 43, no. 4, pp. 879-891, 1994.

[13] C. F. Yang, "A ray-tracing method for modeling indoor wave propagation and penetration," *IEEE Transactions on Antennas and Propagation*, vol. 46, no. 6, pp. 907-919, 1998.

[14] R. G. Kouyoumjian and P. H. Pathak, "A uniform theory of diffraction for an edge in a perfectly conducting surface," *Proc. IEEE*, vol. 62, no. 4, pp. 1448-1462, 1974.

[15] G. Gennarelli and G. Riccio, "A uapo-based model for propagation prediction in microcellular environments," *Progress in Electromagnetics Research B*., vol. 17, pp. 101-116, 2009.

[16] H. W. Son and N. H. Myung, "A deterministic ray tube method for microcellular wave propagation prediction model," *IEEE Trans. Antennas and Propag.*, vol. 47, no. 8, pp. 1344-1350, 1999.

[17] A. Tayebi, J. Gómez, F. S. de Adana and O. Gutierrez, "The application of arrival and received signal strength in multipath indoor environments," *Progress In Electromagnetics Research*, vol. 91, pp. 1-15, 2009.

[18] H. B. Song, H. G. Wang, K. Hong and L. Wang, "A novel source localization scheme based on unitary esprit and city electronic maps in urban environments," *Progress In Electromagnetics Research*, vol. 94, pp. 243-262, 2009.

[19] H. Ling, R. C. Chou and S. W. Lee, "Shooting and bouncing rays: calculating the RCS of an arbitrarily

shaped cavity," *IEEE Transactions on Antennas and Propagation*, vol. 37, pp. 194-205, 1989.
[20] F. Weinmann, "Ray tracing with PO/PTD for RCS modeling of large complex objects," *IEEE Transactions on Antennas and Propagation*, vol. 54, nº. 6, pp. 1797-1806, 2006.
[21] T. Griesser and C. A. Balanis, "Backscatter analysis of dihedral corner reflectors using physical optics and the physical theory of diffraction," *IEEE Transactions on Antennas and Propagation*, vol. 35, pp. 1137-1147, October 1987.
[22] F. Weinmann, "UTD shooting-and-bouncing extension to a PO/PTD ray tracing algorithm," *Applied Computational Electromagnetics Society Journal*, vol. 24, nº. 3, pp. 281-293, 2009.
[23] J. P. Rossi and Y. Gabillet, "A mixed ray launching/tracing method for full 3-D UHF propagation modeling and comparison with wide-band measurements," *IEEE Transactions on Antennas and Propagation*, vol. 50, nº. 4, pp. 517-523, 2002.
[24] B. Choudhury, H. Singh, J. P. Bommer and R. M. Jha, "RF field mapping inside a large passenger-aircraft cabin using a refined ray-tracing algorithm," *IEEE Antennas and Propagation Magazine*, vol. 55, nº. 1, pp. 276-288, 2013.
[25] L. Azpilicueta, F. Falcone, J. J. Astráin, J. Villadangos, I. J. García Zuazola, H. Landaluce, I. Angulo and A. Perallos, "Measurement and modeling of a UHF-RFID system in a metallic closed vehicle," *Microwave and Optical Technology Letters*, vol. 54, issue 9, pp. 2126-2130, 2012.
[26] J. A. Nazábal, P. López Iturri, L. Azpilicueta, F. Falcone and C. Fernández-Valdivielso, "Performance analysis of IEEE 802.15.4 compliant wireless devices for heterogeneous indoor home automation environments," *International Journal of Antennas and Propagation*, Hindawi Publishing Corporation, 2012.
[27] S. Led, L. Azpilicueta, E. Aguirre, M. Martínez de Espronceda, L. Serrano and F. Falcone, "Analysis and description of HOLTIN service provision for AECG monitoring in complex indoor environments," *Sensors*, vol. 13, issue 4, pp. 4947-4960, 2013.
[28] P. López Iturri, J. A. Nazábal, L. Azpilicueta, P. Rodriguez, M. Beruete, C. Fernández-Valdivielso and F. Falcone, "Impact of high power interference sources in planning and deployment of wireless sensor networks and devices in the 2.4 GHz frequency band in heterogeneous environments," *Sensors*, vol. 12, issue 11, pp. 15689-15708, 2012.
[29] A. Cardama Aznar, "Antenas," *Edicions UPC*, 1993.
[30] H. D. Hristov, "Fresnel zones in wireless links, zone plate lenses and antennas," *Artech House, Inc.*, 2000.
[31] Recomendattion UIT-R, p. 526-11, s. l., "Propagación por difracción, serie p. propagación de las ondas radioeléctricas," October 2009.
[32] R. J. Luebbers, "A heuristic UTD slope diffraction coefficient for rough lossy wedges," *IEEE Transactions on Antennas and Propagation*, vol. 37, pp. 206-211, 1989.
[33] R. J. Luebbers, "Comparison of lossy wedge diffraction coefficients with application to mixed path propagation loss prediction," *IEEE Transactions on Antennas and Propagation*, vol. 36, nº. 7, pp. 1031-1034, 1988.
[34] C. A. Balanis, "Advanced engineering electromagnetics," *Wiley New York,* vol. 205, 1989.

Leire Azpilicueta received her Telecommunications Engineering Bachelor degree from the Public University of Navarre (UPNa), Pamplona, Spain in 2009. In 2010, she worked in the R&D department of RFID Osés as a Radio Engineer. In 2011, she obtained her Master of Communications degree held by the Public University of Navarre. She is currently pursuing her Ph.D. degree in Telecommunication Engineering. Her research interests are mobile radio systems, wireless communications and channel modeling.

Meenakshi Rawat (S'09) received her B.Tech. degree in Electrical Engineering from Govind Ballabh Pant University of Agriculture and Technology, Pantnagar, Uttaranchal, India in 2006 and her Ph.D. degree from Schulich School of Engineering, University of Calgary, Calgary, AB, Canada in 2012. She was associated with Telco Construction Equipment Co. Ltd., India from 2006-2007 and Hindustan Petroleum Corporation Limited (HPCL), India during 2007-2008. She is now working with the iRadio Lab of the Schulich School of Engineering, University of Calgary as a as Post-Doctoral-Research fellow. Her current research interests are in the area of digital signal processing, nonlinear filters, artificial neural networks and microwave active and passive nonlinear circuit modeling.

Karun Rawat (M'08, S'09) received his B.E. degree in Electronics and Communication Engineering from Meerut University, UP, India in 2002 and his Ph.D. in Electrical and Computer Engineering, Schulich School of Engineering, University of Calgary, Calgary, AB, Canada in 2012. He worked as a Scientist in the Indian Space Research Organization (ISRO) from 2003-2007. He also worked in iRadio Laboratory of the Schulich School of Engineering, University of Calgary from 2012-2013, where he has been working as a Post Doctoral Research fellow. Currently, he is an Assistant Professor at Indian Institute of Technology, Delhi. He is a Reviewer of several well-known journals. He was also a leader of the University of Calgary team, which won first prize and the best design award in the 3rd Annual Smart Radio Challenge 2010 conducted by Wireless Innovation Forum. His current research interests are in the areas of microwave active and passive circuit design and advanced transmitter and receiver architecture for software defined radio applications

Fadhel M. Ghannouchi is currently a Professor and iCORE/Canada Research Chair with the Department of Electrical and Computer Engineering, Schulich School of Engineering, University of Calgary, Calgary, AB, Canada and Director of the Intelligent RF Radio Laboratory (iRadio Lab). He has held numerous invited positions with several academic and research institutions in Europe, North America and Japan. He has provided consulting services to a number of microwave and wireless communications companies. He has authored or co-authored over 500 publications. He holds ten U.S. patents with five pending. His research interests are in the areas of microwave instrumentation and measurements, nonlinear modeling of microwave devices and communications systems, design of power and spectrum efficient microwave amplification systems and design of intelligent RF transceivers for wireless and satellite communications.

Francisco Falcone (M'05, SM'09) received his Telecommunications Engineering Degree in 1999 and Ph.D. in Communications Engineering in 2005, both at the Universidad Pública de Navarra (UPNA) in Spain. From 1999 to 2000 he worked as Microwave Commissioning Engineer at Siemens-Italtel. From 2000 to 2008 he worked as a Radio Network Engineer in Telefónica Móviles. In 2009 he co-founded Tafco Metawireless, a spin off devoted to complex EM analysis. From 2003 to 2009 he was also Assistant Lecturer at UPNA, becoming Associate Professor in 2009. He has over 280 contributions in journal and conference publications. He has been recipient of the CST Best Paper award in 2003 and 2005, Best Ph.D. in 2006 awarded by the Colegio Oficial de Ingenieros de Telecomunicación, Doctorate award in 2004-2006 awarded by UPNA, Juan Lopez de Peñalver Young Researcher award in 2010 awarded by the Royal Academy of Engineering of Spain and Premio Talgo in 2012 for Technological Innovation. His research area is artificial electromagnetic media, complex electromagnetic scenarios and wireless system analysis.